Understanding the setting and hardening process of wollastonite-based brushite cement. Part 2: Influence of the boron and aluminum concentrations in the mixing solution

Priscillia Laniesse [a,*], Céline Cau Dit Coumes [a], Gwenn Le Saout [b], Adel Mesbah [c]

[a] CEA, DES, ISEC, DE2D, Univ Montpellier, Marcoule, France
[b] LMGC, IMT Mines Alès, Univ Montpellier, CNRS, Alès, France
[c] Institut de Chimie Séparative de Marcoule, ICSM, CEA, CNRS, ENSCM, Univ Montpellier, Marcoule, France

Abstract

The mixing solution of wollastonite-based brushite cement is a phosphoric acid solution containing metallic cations and borax. This work complements a previous study devoted to the influence of the H_3PO_4 concentration, Ca/P and liquid-to-solid (l/s) ratios on the setting and hardening process of the binder by providing new insight into the role of aluminum and boron.

Boron retards the setting and decreases the heat released during the process. It also contributes to reduce the macroporosity of the hardened material but yields to poor compressive strength. With aluminum in the mixing solution, the mechanical properties are greatly improved thanks to the precipitation of an amorphous alumi-nophosphate which increases the density of the cement matrix. But aluminum alone leads to fast setting. A joint addition of boron and aluminum to the mixing solution makes it possible to get a material with optimized properties both in fresh and hardened states.

Keywords:
Hydration
Hydration products
Microstructure
Compressive strength
Chemically bonded ceramics

1. Introduction

Portland cement, possibly blended with fly ash and/or blastfurnace slag, is widely used for nuclear waste encapsulation for several reasons [1–4]. This binder, which has been investigated and used for more than 200 years, is inexpensive and easily available. Properly designed materials usually exhibit good mechanical strength. They are resistant to irradiation at doses of a few MGy representative of those integrated by cemented waste packages over their lifetime. In addition, cement wasteforms are prepared at ambient temperature, using rather simple and robust processes which do not require any special gas treatment. Finally, cement matrices are rather flexible since they can accommodate contaminated effluents, sludges, powders or massive solids. In the first two cases, water brought by the waste can be simply used for cement hydration. As a consequence, cementation is worldwide the reference process for the conditioning of low-level or intermediate-level radioactive waste.

However, Portland cement paste is a very alkaline medium, with a pore solution pH close to 13 [5], which is an issue for the direct stabilization of acidic wastes. Indeed, high temperature rise and flash setting of the grout can result from the fast and exothermic acid-base reaction occurring between protons from the waste and hydroxide ions released by the dissolution of cement phases. Neutralization or basification of such waste before its cementation is thus mandatory [6]. This additional step raises several issues such as *(i)* volume increase resulting from the addition of the base reagent, *(ii)* gelification of the waste due to precipitation of metallic cations (Al^{3+}, Fe^{3+}, Zn^{2+}…) as hydroxides, which makes its transfer to the cementation unit difficult and can lead to poorly workable grout [7], and *(iii)* enhanced risk of alkali-silica reaction in the long term if the pre-treatment solution is a concentrated solution of sodium or potassium hydroxide and if the aggregates used in the concrete formulation are not carefully selected [8,9].

To overcome these issues and suppress the pre-treatment step, an alternative strategy may be to use a binder showing better chemical compatibility with acidic wastes than Portland cement [10]. In this way, wollastonite-based brushite cement is a potential candidate as its setting and hardening process occurs in acidic medium (between 0 and 6) [11–13]. This binder is prepared by mixing wollastonite, a natural metasilicate ($CaSiO_3$), with a solution containing phosphoric acid, borax and metallic cations [14,15]. In a previous paper [16], the authors have

showed that the hydration of wollastonite with a commercial mixing solution comprising broax, zinc and aluminum cations is a multi-step process which involves the formation of a transient crystalline phase (Monocalcium phosphate monohydrate $Ca(H_2PO_4)_2{\cdot}H_2O$ (MCPM)), and produces brushite ($CaHPO_4{\cdot}2H_2O$) as well as an amorphous alumino-phosphate phase containing zinc and calcium. However, data about the influence of the mixing solution composition on the properties of the resulting material are scarce in the literature. A previous work [17] was focussed on the impact of the phosphoric acid concentration, Ca/P molar ratio and liquid-to-solid (l/s) ratio. Increasing the Ca/P ratio (at constant H_3PO_4 concentration) and decreasing the l/s ratio were shown to accelerate the early stages of hydration but limited its progress at 7 d. Moreover, basic calcium orthophosphates formed in addition to brushite. At constant l/s ratio, increasing the H_3PO_4 concentration between 7 and 10 mol·L^{-1} delayed cement hydration and inhibited the setting at concentrations above 12 mol·L^{-1}. A good compromise was obtained for H_3PO_4 concentrations within the range 9–10 mol·L^{-1}: setting occurred between 10 and 48 h and the amount of precipitated brushite was at its maximum. However, the sole presence of phosphoric acid in the mixing solution produced materials with poor mechanical strength. Since commercial binders prepared with mixing solutions comprising metallic cations and borax usually have compressive strengths of several tens of MPa [12,13,15], these additions must play a key role in the hardening process of the material. This work investigates their influence into more details.

2. Experimental

2.1. Materials

Wollastonite was provided by the French company Sulitec. The powder comprised wollastonite and small contents of calcite and quartz that were evidenced by XRD and TGA (diagrams are given in [16]). The $CaCO_3$ content was calculated from the weight loss recorded at 654 °C by TGA to be 1.6 ± 0.1 wt%. The particle size distribution of the powder (laser granulometry) was comprised between 0.5 µm and 135 µm (d_{10} = 2.8 µm, d_{50} = 15.2 µm, d_{90} = 48.3 µm). The wollastonite particles had a needle shape with a mean aspect ratio (ratio of the length-to-diameter) close to 4:1 (determined manually using SEM images of c.a. 100 particles).

The mixing solution was a 9 mol·L^{-1} phosphoric acid solution, prepared from 85%wt. H_3PO_4 (14.6 mol·L^{-1}) analytical grade commercial solution provided by VWR.

First, boron and aluminum species were introduced to the phosphoric acid solution separately from each other to investigate their influence on the cement hydration process. Boron was added either as borax ($Na_2B_4O_7{\cdot}10H_2O$) or boric acid ($B(OH)_3$). These two borated species were investigated for the following reasons:

- borax was a cheaper additive,
- boric acid had less influence on the initial acidity of the solution and did not bring any additional cations (Na^+) to the system.

Aluminum was added as metal grade aluminum powder (purity > 99.9%) to the mixing solution. Under such acidic conditions, metallic aluminum is unstable and oxidized into Al^{3+} cations according to Eq. (1).

$$Al + 3H^+ \rightarrow Al^{3+} + 3/2H_2 \quad (1)$$

Al^{3+} cations could thus be produced without any addition of supplementary anions. The temperature rise due to the exothermic nature of reaction (Eq. (1)) and the gas evacuation led to partial evaporation of water which was compensated after complete oxidation of the Al powder by an addition of demineralized water.

Then, the joint effect of aluminum and boron was studied using design of experiments (D.O.E) (cf. Section 2.2).

The addition of each species may have an impact on the acidity of the mixing solution. As the solution was initially very acidic, its pH could not be measured directly with a pH electrode. It was then necessary to determine its Hammett acidity function H_0 [18] Measurement of such function value has been detailed in a previous work [16].

2.2. Specimen preparation

Paste preparation was performed by mixing the powder and solution for 5 min using a laboratory mixer equipped with an anchor stirrer rotating at 250 rpm. Paste samples were then cast into airtight polypropylene boxes (20 mL of paste per box) and cured at 25 ± 1 °C.

At first, the influences of boron and aluminum on the hydration and mechanical properties of the cement paste were investigated separately from each other. Then, to look for possible interactions, boron and aluminum were simultaneously added to the mixing solution.

A first series of cement pastes was thus prepared by varying the concentration (from 0.05 to 0.2 mol·L^{-1}) and the type of boron species in the mixing solution (Table 1). In a second set of experiments, the concentration of aluminum varied from 0.5 to 2.5 mol·L^{-1}. A third series of pastes was formulated with a mixing solution containing various amount of aluminum and borax as described in Section 2.2. In all experiments, the l/s ratio, phosphate concentration and Ca/P ratio were kept constant and respectively equal to 0.76 mL·g^{-1}, 9 mol·L^{-1} and 1.25.

2.3. Experimental design

The combined influence of B and Al on the paste properties was studied using D.O.E [19] to evidence any synergistic or antagonist effects between these two species. The objective was to fit and analyse response surfaces in order to optimize the concentrations of these two additives. The factors (or variables) were the Al (introduced at Al powder) and B (introduced as borax) concentrations in the mixing solution. Their range of variation defined the experimental domain.

- Al: The maximum Al concentration (2.5 mol·L^{-1}) was fixed by the solubility limit of Al^{3+} in the H_3PO_4 solution. Since preliminary experiments with Al^{3+} concentrations of 1 mol·L^{-1} or less led to materials with poor mechanical strength (<1 MPa), the minimum Al concentration was set to 1.5 mol·L^{-1}.
- B: Borax was preferred to boric acid since it had similar retarding effect and was less expensive. The B concentration varied between 0.2 mol·L^{-1} (retardation being too weak for lower concentrations) and 0.6 mol·L^{-1} (the solubility limit in the H_3PO_4 solution).

Coded dimensionless variables varying within the range [−1; 1] were defined according to Eq. (2) (Table 2).

$$\left(\frac{x_j - x_j^0}{\Delta x_j}\right) = \left(\frac{U_j - U_j^0}{\Delta U_j}\right) \quad (2)$$

with x_j = value of coded variable j.

x_j^0 = value of coded variable j at the center of the domain (in this work, $x_j^0 = 0$)
U_j = value of natural variable j
U_j° = value of natural variable j at the center of the domain
$\Delta U_j = \frac{U_j^{max} - U_j^{min}}{2}$
$\Delta x_j = \frac{x_j^{max} - x_j^{min}}{2}$

The P concentration, Ca/P and l/s ratios were maintained constant at 9 mol·L^{-1}, 1.25 (mol/mol) and 0.76 mL·g^{-1} in all runs. The acidity varied however since it depended on the B and Al concentrations.

Table 1
Composition of cement pastes comprising boron (series 1) or aluminum (series 2) or both (series 3) and responses as described in the following section (H_0 stands for the acidity function, the pastes are labelled $P_{BAorB/Y/Z}$ where BA stands for boric acid, B for Borax, Y and Z for the boron and aluminum concentrations respectively).

Exp. number	[Al]	[B]	H_0	R_c	Isothermal calorimetry			BET	Mineralogy at 28 d		
	mol·L^{-1}	mol·L^{-1}		MPa	t_{max} (h)	HF_{max} (mW/g)	H_{max} (J/g)	d_p (Å)	Wollastonite (wt%)	Brushite (wt%)	Amorphous (wt%)
Reference											
$P_{0/0}$	0	0	−1.85	<1	11.9	68.5	738	–	–	–	–
Series 1											
$P_{B/0.05/0}$	0	0.05	−1.87	<1	26.8	27.8	712	–	–	–	–
$P_{B/0.2/0}$	0	0.2	−1.87	<1	74.6	6.9	603	–	–	–	–
$P_{BA/0.05/0}$	0	0.05	−1.87	<1	24.8	28.7	716	–	–	–	–
$P_{BA/0.2/0}$	0	0.2	−1.87	<1	82.0	8.8	625	–	–	–	–
Series 2											
$P_{0/0.5}$	0.5	0	−1.61	2.1	6.9	55.0	634	–	–	–	–
$P_{0/1.0}$	1.0	0	−1.45	6.5	6.5	48.7	580	–	–	–	–
$P_{0/2.0}$	2.0	0	−1.41	13.9	5.2	38.6	497	–	–	–	–
$P_{0/2.5}$	2.5	0	−1.35	69.8	9.6	35.2	486	–	–	–	–
Series 3											
$P_{B/0.2/1.5}$	1.5	0.2	−1.43	30.6	17.6	10.7	537	54.0	10.4	52.9	12.5
$P_{B/0.2/2.5}$	2.5	0.2	−1.35	57.5	10.2	15.5	438	40.9	10.1	34.3	31.5
$P_{B/0.6/1.5}$	1.5	0.6	−1.44	35.6	43.5	3.0	492	66.4	17.2	55.3	6.6
$P_{B/0.6/2.5}$	2.5	0.6	−1.34	55.8	19.3	5.9	415	44.6	17.7	35.5	26.5
$P_{B/0.4/1.5}$	1.5	0.4	−1.43	30.8	29.8	5.4	496	59.4	15.7	51.9	10.9
$P_{B/0.4/2.5}$	2.5	0.4	−1.34	47.7	13.5	9.9	431	40.6	14.7	35.2	28.3
$P_{B/0.2/2.0}$	2.0	0.2	−1.41	40.5	12.9	12.8	493	46.4	12.0	47.8	16.7
$P_{B/0.6/2.0}$	2.0	0.6	−1.40	45.6	29.0	4.3	451	51.9	15.3	43.4	19.6
$P_{B/0.4/2.0-1}$	2.0	0.4	−1.41	45.5	21.1	7.2	460	47.4	15.2	50.3	12.5
$P_{B/0.4/2.0-2}$	2.0	0.4	−1.41	36.5	20.7	7.2	482	51.2	12.2	45.8	18.7
$P_{B/0.4/2.0-3}$	2.0	0.4	−1.41	46.1	20.6	7.4	467	47.4	11.0	41.0	24.4
$P_{B/0.4/2.0-4}$	2.0	0.4	−1.41	43.9	21.5	7.0	461	49.6	12.7	47.9	16.4

Table 2
Correspondence between natural and coded variables.

Factor	Natural variables		Coded variables	
	Notation	Range of variation (mol·L^{-1})	Notation	Range of variation
[Al]	U_1	[1.5; 2.5]	X_1	[−1; 1]
[B]	U_2	[0.2; 0.6]	X_2	[−1; 1]

Eight responses were measured in order to characterize the cement hydration rate, the mineralogical assemblage and compressive strength of pastes after 28 d of curing in sealed bag at 25 °C. More precisely, the cement hydration, investigated by isothermal calorimetry, was characterized by the maximum heat flow, the corresponding time and the maximum cumulative heat. The phase assemblage was characterized by XRD and calculated quantitatively by Rietveld refinement in order to quantify the amount of brushite, wollastonite and amorphous aluminophosphate at a 28 days. Finally, the compressive strength and the mean diameter of pores were measured in order to characterize and explain mechanical performances of the binders. More details are given in Section 2.4.

Since the objective of the study was to predict response values within the experimental domain, the postulated empirical model was a quadratic polynomial (Eq. (3)).

$$y = \beta_0 + \beta_1 x_1 + \beta_2 x_2 + \beta_{11} {x_1}^2 + \beta_{22} {x_2}^2 + \beta_{12} x_1 \cdot x_2 + \varepsilon \quad (3)$$

with: y = predicted response, x_i = level of factor X_i, β_i = model coefficient to be estimated, and ε = error.

The positioning of experimental points within the experimental domain is of great importance to obtain a good precision on the estimates of the model parameters and on the model-predicted response values. The selected design was a face-centered central composite design ($\alpha = 1$) [20] comprising 9 experiments located at the corners, center and edge centroids of the experimental domain (Fig. 1). This design exhibits interesting properties such as limited number of trials and good quality

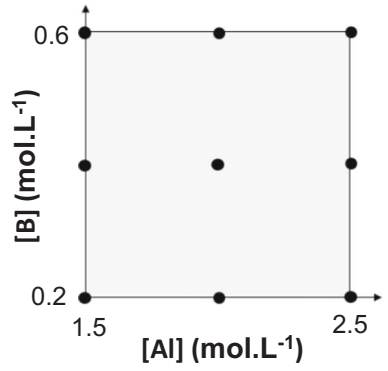

Fig. 1. Positioning of the experiments within the experimental design.

of predicted response values (maximum prediction variance d_{max} of 0.81 over the domain of interest, meaning that, if the model is validated, the variance of predicted response is $\leq 0.81\ \sigma^2$, where σ^2 is the experimental variance). The experiment at the center of the domain was repeated 3 times to assess the variance of the experimental error. Table 3 summarizes the experimental design and the measured response values (see Section 2.3 for the characterization methods used).

Table 3
ICDS files associated to crystalline phase.

Crystalline phase	ICDS file
Brushite	72-0713
Wollastonite	84-0654
Quartz	70-7344
Silicon	27-1402
MCPM	09-0347

2.4. Characterization techniques

The hydration process of the cement pastes was characterized using a TAM AIR conduction microcalorimeter under isothermal conditions at 25 °C. The pastes samples were prepared outside the calorimeter. About 2 g were poured into a glass ampoule and introduced in the calorimeter (more details about the technique are given in [16]).

A typical curve obtained by this technique is given in Fig. 2. Three parameters were extracted for further analysis:

- the maximum heat flow (HF_{max}): the higher the heat flow, the faster the dissolution of wollastonite which was the main exothermic reaction in the hydration process [16],
- the time corresponding to the maximum heat flow (t_{max}), which gave information on the setting time of the material (previous experiments showed that it approximately corresponded to the end of setting [16]) and on the duration of the low thermal activity period that preceded the peak,
- the cumulative heat (H_{max}), which provided insight into the self-heating behaviour of the material during hydration and strongly depended on the progress of exothermic reactions. Note that the first 30 min were omitted for H_{max} calculation due to extra undesirable heat resulting from the introduction of the ampoule in the calorimetric chamber.

The hydration process of paste samples was stopped by successively immersing the crushed paste into isopropanol for few minutes, filtrating the suspension and drying it in an oven at 38 °C for 24 h. Preliminary trials showed that the drying at 38 °C for 24 h had no effect on the samples mineralogy.

The phase assemblage was analysed using XRD in a Debbye Scherrer configuration (transmission mode) according to the procedure described in [16]. To reduce the preferred orientation effect, the samples, ground to a particle size less than 80 μm and containing 10 wt% Si used as an internal standard, were introduced in Lindeman tubes (0.7 mm by diameter) and mounted on a spinning goniometric head. Measurement was performed using the Debye Scherrer configuration (transmission mode) with copper radiation (λ = 1.5418 Å) at room temperature in the 2θ range 5–120° (step size of 0.017°, total counting time of 6 h). Refinement of the X-ray diagrams was then performed using the Rietveld method. The internal standard method made it possible to calculate the amount of amorphous phases as explained in [16]. Calculations were carried out using the Fullproof_suite software [21]. ICDS files used for the assignment of crystalline phases are given in Table 3.

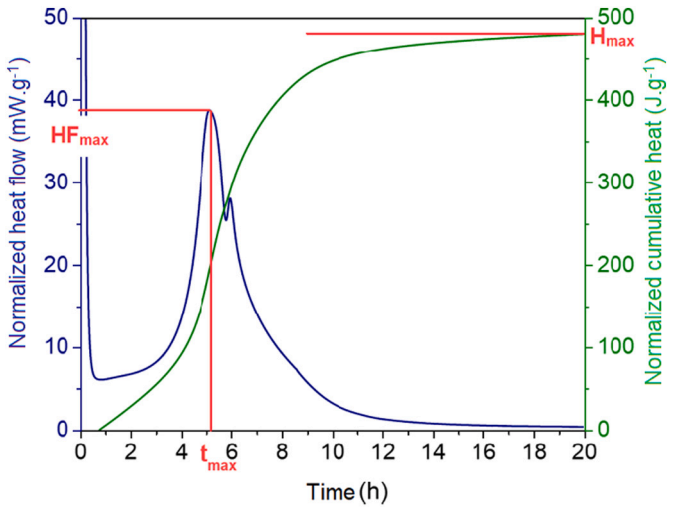

Fig. 2. Typical curves obtained (experiment $P_{0/2.0}$) by isothermal microcalorimetry and parameters used for their analysis.

The mechanical strength of 4 × 4 × 4 cm paste specimens was characterized after 28 d of curing at 25 °C in a sealed bag (endogenous conditions). The compressive strength was measured following EN 196-1 European standard (loading rate: 2.4 $kN{\cdot}s^{-1}$) with the 3R RP 40/400FC testing machine.

Polished fractions of paste samples were observed by Scanning Electron Microscopy (FEI Inspect S50, high vacuum mode, acceleration voltage of 15 kV, current intensity of 50 nA, working distance of 9.7 mm). More details about the polishing protocol are given in [16]. Elemental mapping was performed using X-ray microanalysis (high vacuum mode, Bruker X-flash SDD detector (10 mm^2)). The Ca/P, Al/P and Zn/P ratios in the hydrates were determined with statistics on 20 to 30 measurement points, after calibration of the detector using jadeite for Na, aluminum metal for Al, zinc metal for Zn, GaP for P and wollastonite for Si and Ca.

The pore structure (in the range of mesopores) was characterized using the nitrogen adsorption technique. Samples were first freeze-dried, and then stored for 12 h under vacuum at 75 °C to remove the water and gas impurities adsorbed on the pores surface. Preliminary characterizations by XRD showed that this drying procedure did not change the mineralogy of the samples. Gas sorption experiments were performed using Micromeritics ASAP 2020 device. Analyses were carried out at the liquid nitrogen temperature (77 K) with a relative pressure ranging from 5.10^{-6} to 0.99. The pore size distribution was determined using the Barret-Joyner-Halenda (BJH) method.

3. Results and discussion

3.1. Influence of the type and concentration of boron-containing species (first series of experiments)

3.1.1. Hydration rate

At a given boron concentration, boric acid and borax had almost the same effect on the cement hydration rate (Fig. 3). The higher the boron concentration, the higher the time corresponding to the maximum heat flow, and the longer the duration of the low thermal activity, meaning that boron retarded the hydration process. Moreover, whereas the heat flow curve of the reference paste sample exhibited one main peak, three thermal events were evidenced in the presence of boron, as previously observed for commercial cement pastes having more complex mixing solution (additional presence of Zn and Al cations) [16]. The maximum heat flow was reduced from 72 to 7 $mW{\cdot}g^{-1}$ when the boron concentration was increased from 0 to 0.2 $mol{\cdot}L^{-1}$. This heat flow value was close to that of commercial products [16].

Pastes prepared with 0 and 0.05 $mol{\cdot}L^{-1}$ of boron displayed the same cumulative heat at the end of the experiment, suggesting similar progress of hydration. For higher boron concentrations, the plateau was not reached at the end of experiment, making the cumulative heat flows difficult to compare.

3.1.2. Phase assemblage

The phase evolution of pastes $P_{B/0.05/0}$ and $P_{BA/0.05/0}$ was characterized by XRD. Regardless of the boron additive, MCPM precipitated rapidly after mixing and was destabilized to form brushite after the heat flow peak. The precipitation sequence was thus similar to that evidenced for the commercial binder [16] (Fig. 4):

Even if the hydration process was slowed down, wollastonite was almost totally consumed at 48 h. Brushite ($CaHPO_4.2H_2O$) precipitated instead of monetite ($CaHPO_4$), the product observed for the boron-free reference [17]. This result could be explained by the lower self-heating of the boron-containing material which tended to promote the precipitation of metastable brushite instead of thermodynamically stable monetite [22].

The main role of boron was to delay the hydration and reduce the maximum heat flow. The X-Ray diffraction results showed that boron mainly influenced the conversion of MCPM to brushite which occurred

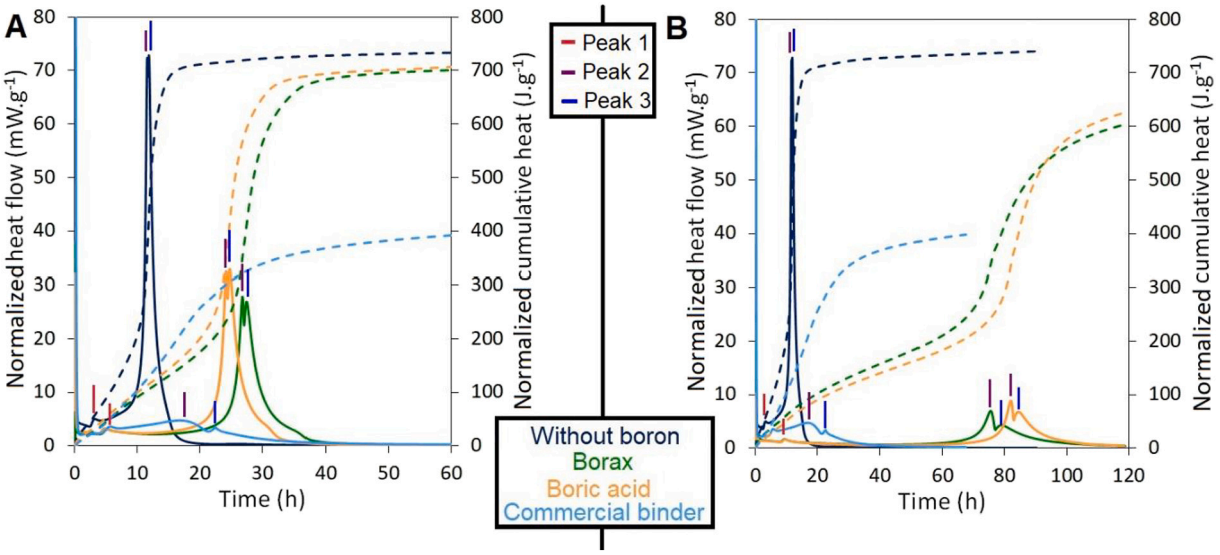

Fig. 3. Normalized heat flow and cumulative heat of cement pastes prepared with various concentrations of boron (A: 0.05 mol·L^{-1}; B: 0.2 mol·L^{-1}) introduced as borax or boric acid.

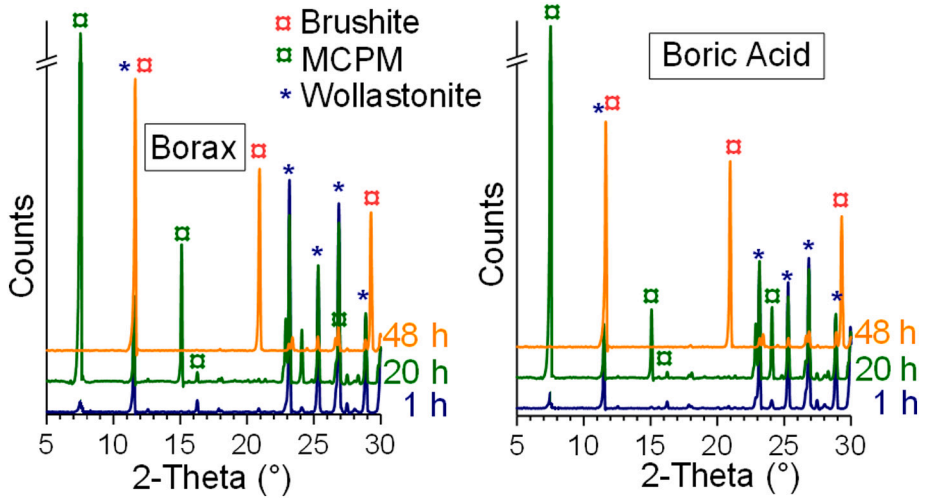

Fig. 4. X-Ray diffraction patterns (background subtracted) of paste samples prepared with 0.05 mol·L^{-1} of boron, added as borax (left) or boric acid (right).

later as compared to the MCPM-monetite transition evidenced in the boron-free reference paste [17]. The retarding effect of boron could thus result from a delay in MCPM dissolution and/or brushite precipitation.

3.1.3. *Mechanical properties*

All the paste samples containing boron ($P_{B/0.05/0}$, $P_{BA/0.05/0}$, $P_{B/0.2/0}$, $P_{BA/0.2/0}$) had a very poor compressive strength (< 1 MPa, the lower limit of the measurement range of the testing machine) at 28 d. Moreover, their free surface exhibited a dome, indicating a strong volume instability.

3.2. *Influence of the aluminum concentration (second series of experiments)*

3.2.1. *Hydration rate*

Increasing the aluminum concentration in the mixing solution from 0 to 2.5 mol·L^{-1} decreased the length of the low thermal activity period, the maximal heat flow and cumulative heat (Fig. 5). However, the heat flow reduction was much less important than in the presence of boron. It must be kept in mind that increasing the Al concentration also decreased

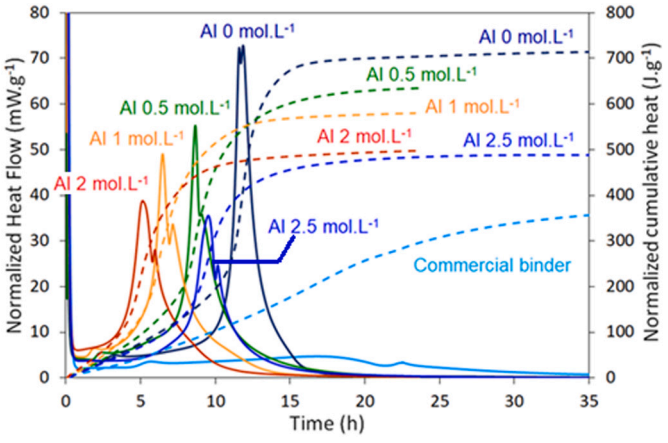

Fig. 5. Heat flow (solid lines) and cumulative heat (dotted lines) of pastes prepared with different concentrations of aluminum in the mixing solution.

the acidity of the mixing solution (see Eq. (1)). In a previous work, it was shown that decreasing the acidity (or, equivalently, increasing the acidity function H_0 within the range [−2.13, −1.28]) decreased the period of low thermal activity and cumulative heat but increased the maximal heat flow [17]. Consequently, the reduction in the maximal heat flow observed with increasing [Al^{3+}] could not be attributed to an acidity effect, but to the presence of metallic cations. As for the variation of the cumulative heat and duration of the period of low thermal activity, both parameters (acidity and [Al^{3+}]) could be involved. The evolution of the cumulative heat was plotted versus the acidity function and compared to the curve obtained for solutions containing phosphoric acid only [17] (Fig. 6). For low aluminum concentrations, the effect of the acidity seemed to be predominant, whereas, for Al concentrations higher than 1 mol·L^{-1}, the decrease in the acidity resulting from the introduction of aluminum to the mixing solution could not explain by itself the decrease in the cumulative heat, meaning that Al^{3+} cations were also involved. Paste $P_{0/2.5}$ seemed to show a distinct behaviour, with a period of low thermal activity intermediate between those of pastes $P_{0/0}$ and $P_{0/2.}$ Complementary experiments would be needed to clarify this point.

3.2.2. *Phase assemblage*

The mineralogy of paste $P_{0/2}$ prepared with 2 mol·L^{-1} of aluminum was characterized by XRD at relevant hydration times: 1 h (period of low thermal activity), 5 h (maximum of the heat flow), 8 h (end of the second peak) and 48 h (Fig. 7).

The presence of MCPM was evidenced shortly after mixing. Its amount seemed to increase until the first heat flow peak. Then, this phase was destabilized and brushite precipitated. Wollastonite was not totally depleted at 48 h. Residual wollastonite (in orange) even persisted after 28 d, as shown by the elemental mapping performed on a polished section of paste P0/2.5 (Fig. 8). Silica (in green) was detected at the initial location of wollastonite grains, suggesting an incongruent dissolution of wollastonite as observed previously [16,23,24]. The presence of brushite was also clearly evidenced (zones in purple with intense colour). In addition, EDS mapping and EDS spectra (Fig. 9) showed the precipitation of a phase containing Al, P and Ca (in light purple). This phase, which was not detected by XRD, was likely amorphous or poorly crystalline (Fig. 8). Similarly, precipitation of an amorphous aluminophosphate phase containing calcium and zinc was reported for a commercial binder prepared with a mixing solution comprising

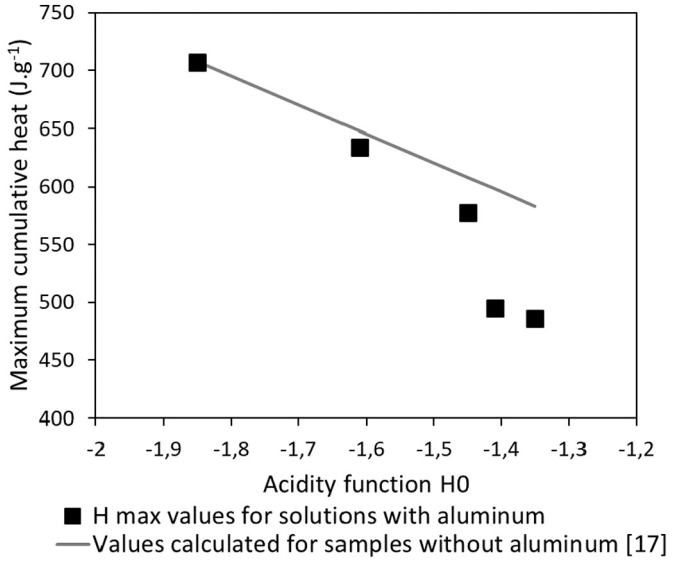

Fig. 6. Evolution of the cumulative heat in function of the solution acidity – comparison with values obtains for solutions containing only phosphoric acid from [17].

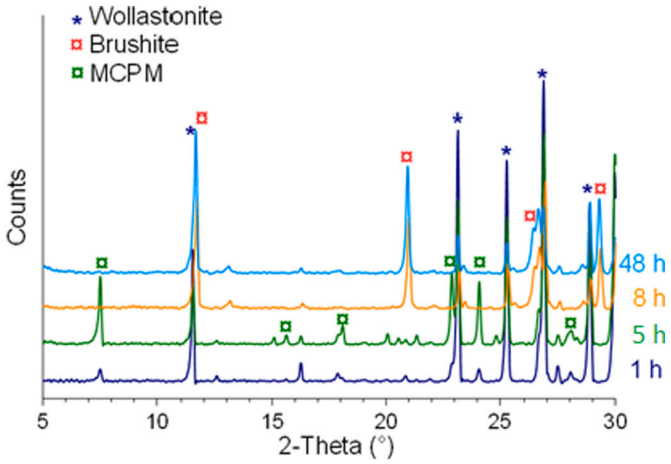

Fig. 7. X-Ray diffraction patterns (background subtracted) of paste $P_{0/2}$ prepared with 2 mol·L^{-1} of aluminum after 1 h to 48 h of hydration.

aluminum and zinc cations [16].

3.2.3. *Mechanical properties*

The compressive strength of 28 d-old paste samples increased from less than 1 MPa (reference paste $P_{0/0}$ – [Al^{3+}] = 0 mol·L^{-1}) to 14 MPa (Paste P0/2 - [Al^{3+}] = 2 mol·L^{-1}) and 52 MPa (Paste P0/2.5 - [Al^{3+}] = 2.5 mol·L^{-1}). The aluminum concentration thus seemed to have an outstanding effect on the mechanical properties of the hardened material. Note that the strength increase with the aluminum concentration could not be explained by the decrease in acidity since all the pastes prepared with Al-free mixing solutions of variable acidity exhibited a compressive strength less than 1 MPa [17]. In addition, visual observation showed that unlike the hardened pastes with boric acid or borax, those with aluminum did not show any expansion.

3.2.4. *Discussion about the influence of aluminum on the rate of hydration*

Increasing the Al concentration reduced the period of low thermal activity, but also the cumulative heat flow. This effect could be partly explained by the decreased acidity of mixing solutions with high Al concentrations, but the contribution of aluminum was also evidenced.

The presence of aluminum changed the mineralogical assemblage formed by hydration since an amorphous aluminophosphate phase precipitated in addition to MCPM and brushite or monetite. It was evidenced from the first characterization time, in good agreement with previous observations [16]. The rapid precipitation of this amorphous phase consumed ions from the solution, which in turn could promote the dissolution of wollastonite and decrease the period of low thermal activity.

The cumulative heat decreased however in the presence of aluminum, which indicated a smaller extent of dissolution of wollastonite since this process was shown to govern the heat production [17]. Increasing the Al concentration likely favoured the precipitation of the aluminophosphate phase (this will be shown in Section 3.3 for pastes prepared with mixing solutions containing B ad Al), which resulted in a denser microstructure, evidenced by the SEM observations and higher mechanical strength. This denser microstructure might contribute to slowing down the subsequent progress of hydration because of a more difficult access to wollastonite or water, or a lack of space for the precipitation of hydrates.

3.3. *Joint influence of aluminum and boron concentrations (third series of experiments)*

The joint influence of the Al and B concentration in the mixing solution on the paste properties was investigated using the experimental

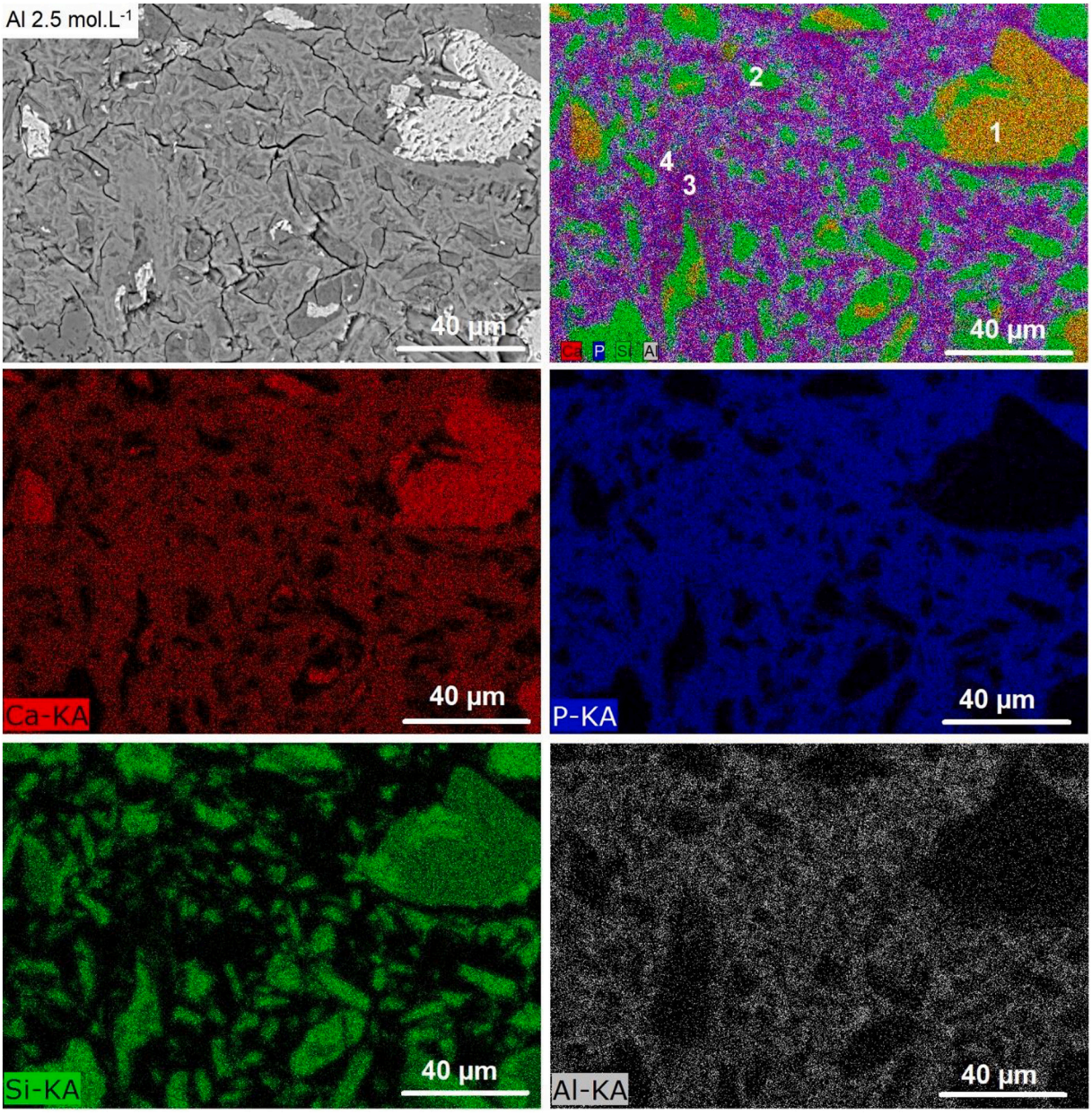

Fig. 8. SEM image (BSE, WD 9.7 mm, 15 kV) and elemental mapping of a polished section of paste $P_{0/2.5}$ prepared with 2.5 mol·L^{-1} of aluminum and cured for 28 days in sealed bag at 25 °C (1: wollastonite; 2: amorphous silica; 3: brushite; 4: amorphous aluminum phosphate).

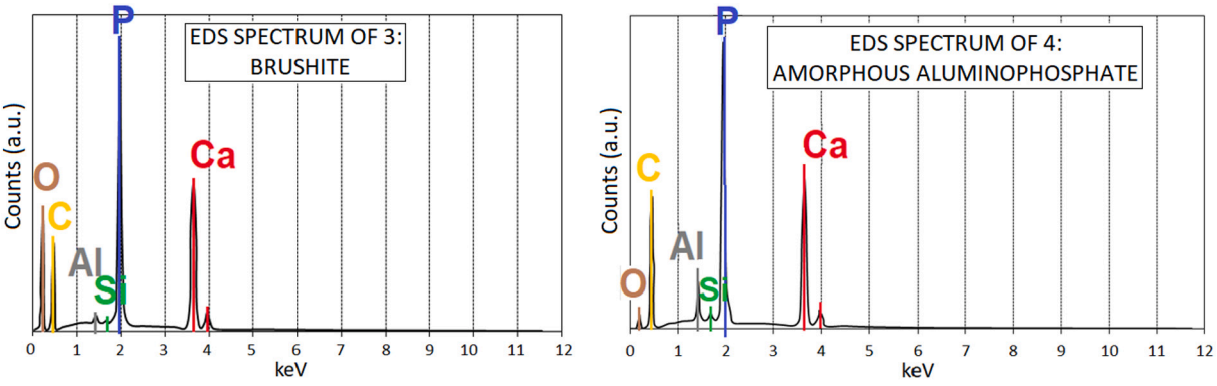

Fig. 9. X-ray microanalysis in spots 3 and 4 of Fig. 8: brushite (left) and calcium aluminophosphate (right).

design shown in Table 1. For each response, the model coefficients were estimated from the results by standard least squares regression using the Nemrod software [25] (Table 4). Possible model deficiencies were looked for by analysis of variance [26] (Table 5). The variance of the experimental error was first estimated using the replicated runs. Since there were degrees of freedom to calculate the residuals, model adequacy was then checked by verifying that the lack of fit of the model was statistically not significant. Finally, a test for significance of regression was carried out by assuming that all coefficients β_i were zero. Rejection of this hypothesis implied that at least one of the regressor variables x_i contributed significantly to the model, and that this model was thus meaningful. Validated models could be built for all the responses (Table 5), with predictive power ranging from good (H_{max}, Amorphous, Brushite, R_c) to excellent (HF_{max}, t_{max}, d_p), as indicated by the R^2_{pred} values (Table 4). Note that, for response "%wt Amorphous", one replicate run ($P_{B/0.4/2.0}$–3), characterized by a residual almost twice that of the experimental error, was considered as erratic and discarded for the calculation of the model.

3.3.1. Hydration rate

The contour plots for responses HF_{max}, t_{max} and H_{max} (Fig. 10) showed that both boron and aluminum affected the cement hydration rate. Indeed, the higher the boron concentration, the lower the maximum heat flow and the higher the corresponding hydration time t_{max}. In addition, increasing the boron concentration slightly decreased the maximum cumulative heat. Therefore, boron kept its retarding effect in the presence of aluminum. As for aluminum, raising its concentration strongly decreased t_{max}, and thus the duration of the low thermal activity period, as well as the maximum cumulative heat, and increased to a minor extent the maximum heat flow. Thus, in the presence of boron, aluminum still accelerated the first stages of hydration and limited its progress afterwards. Its influence on the maximum heat flow changed however, since this parameter was shown to decrease when the Al concentration increased in the absence of boron (cf Section 3.2.1). From a methodological point of view, this change of behaviour indicated the existence of an interaction between the two factors [Al] and [B]. Complementary investigations would be needed to explain its origin from a phenomenological point of view.

3.3.2. Mineralogy

The mass fractions of wollastonite, brushite and amorphous phase in 28 d-old cement pastes were estimated using Rietveld refinement.

The mass fraction of residual wollastonite did not evolve significantly as a function of the mixing solution composition. The observed variations were of the same magnitude order as the experimental error estimated from the replicates.

In contrast, the fractions of brushite and amorphous phase strongly depended on the aluminum concentration in the mixing solution (Fig. 11). The higher this concentration, the higher the content of amorphous phase and the lower that of brushite. The boron concentration had comparatively very little influence. It is interesting to note that, within all the investigated experimental domain, the fraction of brushite remained much higher – and that of the amorphous phase much lower - than those of a binder prepared with the same wollastonite powder, but with a mixing solution additionally containing zinc at a concentration of 1.3 mol·L^{-1} [16]. This latter comprised indeed 21 wt% brushite and 48 wt% amorphous phase at the same age. Therefore, the presence of zinc in the mixing solution seemed to inhibit the formation of brushite and promote the formation of amorphous phase. This hypothesis is supported by previous work showing the inhibiting effect of zinc onto brushite crystallization [27].

The amorphous phase present in samples $P_{B/0.6/1.5}$ and $P_{B/0.6/2.5}$ (mixing solution containing 0.6 mol·L^{-1} of boron and 1.5 or 2.5 mol·L^{-1} of aluminum) was studied by SEM-EDS after 28 d of curing in sealed bag. Elemental mapping showed that the amorphous phase (in light purple on Fig. 12) was more dispersed in the aluminum-rich sample. Moreover, its composition varied as a function of the initial amount of aluminum: Al concentration of 1.5 mol·L^{-1} and 2.5 mol·L^{-1} yielded Ca/P ratios of 0,53 ± 0,03 and 0,86 ± 0,08 respectively, and Al/P ratios of 0,54 ± 0,02 and 0,4 ± 0,1 respectively. The higher Ca/P ratio of the amorphous phase in sample $P_{B/0.6/2.5}$ was consistent with its lower brushite content (the amount of depleted wollastonite being approximatively the same in both pastes, calcium ions precipitated in the amorphous phase preferentially to brushite). Nevertheless, it cannot be excluded that this higher Ca/P ratio also resulted from a submicronic mix of brushite with the better dispersed amorphous phase. On the contrary, the Al/P ratio was slightly lower, which could arise from the higher content of amorphous phase formed during the hydration process.

3.3.3. Compressive strength

The aluminum concentration in the mixing solution not only influenced the phase assemblage of the hardened cement paste, but also its mechanical strength (Fig. 13). Increasing this concentration from 1.5 to 2.5 mol·L^{-1} almost doubled the compressive strength. With Al concentrations above 2.2 mol·L^{-1}, the paste samples exhibited higher strength than the commercial binder investigated in [16]. The boron concentration was much less influent. However, raising its value within the range 0.4–0.6 mol·L^{-1} also tended to improve slightly the compressive strength. It was shown in Section 3.3.2 that increasing the Al concentration promoted the precipitation of the amorphous alumino-phosphate phase at the expense of brushite. This amorphous phase thus seemed to play a key role in the strength development of the material because it had better binding properties than brushite and/or led to denser microstructure.

Observation by SEM of polished cross sections of $P_{B0.2/1.5}$, $P_{B0.2/2.5}$, $P_{B0.6/1.5}$ and $P_{B0.6/2.5}$ samples prepared with mixing solutions containing 0.2 or 0.6 mol·L^{-1} of boron and 1.5 or 2.5 mol·L^{-1} of aluminum showed that these two species had not the same effect on porosity (Fig. 14). Pastes prepared with the highest Al concentration showed a denser cement matrix, but also a higher macroporosity. Note that this latter mainly resulted from CO_2 release within the paste due the destabilization in acidic medium of calcite present as traces in the wollastonite powder. Evacuation of the gas bubbles from the fresh paste was likely more difficult at high Al concentration since setting occurred faster.

Table 4
Estimated coefficients of polynomial models for the different investigated responses.

Response	HF_{max}	t_{max}	H_{max}	brushite	Amorphous	R_c	d_p
Unit	mW/g	h	J/g	wt%	wt%	MPa	Å
b_0	7.250	20.814	466.057	46.022	16.784	41.750	48.981
b_1	2.032	−7.978	−40.225	−9.171	9.392	10.667	−8.953
b_2	−4.275	8.529	−18.342	−0.157	−1.337	1.400	3.587
b_{11}	0.327	1.169	–	−1.851	2.601	–	1.988
b_{22}	1.226	0.477	5.086	–	–	2.517	–
b_{12}	−0.460	−4.230	5.646	–	–	–	−2.178
R^2	0.998	0.998	0.960	0.890	0.917	0.864	0.973
R^2_A	0.997	0.996	0.937	0.848	0.881	0.813	0.958
R^2_{pred}	0.988	0.985	0.862	0.800	0.806	0.725	0.912

Table 5
Checking for accuracy and significance of models using ANOVA.

Response	Source	Sum of squares	df	Mean squares	F-test	P-value
HF_{max}	Regression	140.9352	5	28.1870	701.2372	<0.01***
	Residuals	0.2412	6	0.0402		
	Lack of fit	0.1651	3	0.0550	2.1696	27.1
	Replication error	0.0761	3	0.0254		
	Total	141.1764	11			
t_{max}	Regression	895.9243	5	179.1849	540.8123	<0.01***
	Residuals	1.9880	6	0.3313		
	Lack of fit	1.4230	3	0.4743	2.5190	23.4
	Replication error	0.5649	3	0.1883		
	Total	897.9122	11			
H_{max}	Regression	1.193E + 04	4	2.983E+003	41.57	<0.01***
	Residuals	5.023E + 02	7	7.176E+01		
	Lack of fit	2.011E + 02	4	5.029E+01	0.501	74.3
	Replication error	3.012E + 02	3	1.004E+02		
	Total	1.243E + 04	11			
wt% brushite	Regression	515.0152	3	171.6717	21.5293	0.0347***
	Residuals	63.7908	8	7.9739		
	Lack of fit	17.0748	5	3.4150	0.2193	93.2
	Replication error	46.7160	3	15.5720		
	Total	578.8060	11			
wt% amorphous	Regression	558.4234	3	186.1411	25.7816	0.0371***
	Residuals	50.5394	7	7.2199		
	Lack of fit	30.9680	5	6.1936	0.6329	70.6
	Replication error	19.5714	2	9.7857		
	Total	608.9628	10			
R_c	Regression	713.4275	3	237.8092	16.9801	0.0789***
	Residuals	112.0417	8	14.0052		
	Lack of fit	53.1217	5	10.6243	0.5410	74.4
	Replication error	58.9200	3	19.6400		
	Total	825.4692	11			
d_p	Regression	588.9969	4	147.2492	63.9925	<0.01***
	Residuals	16.1073	7	2.3010		
	Lack of fit	5.7032	4	1.4258	0.4111	79.5
	Replication error	10.4041	3	3.4680		
	Total	605.1041	11			

P-value: probability that a random variable having a F-distribution is greater than the F-test; ***: P < 0.1%.

Increasing the boron concentration from 0.2 to 0.6 mol·L^{-1} decreased the macroporosity since the gas bubbles were filled with brushite crystals. This observation suggests that, in the presence of boron, calcium ions released by the dissolution of wollastonite could diffuse within the matrix before precipitating. This filling of macropores may explain the beneficial effect on the compressive strength evidenced at high boron concentrations.

Finally, aluminum and boron were shown to have opposite effects on the mean mesopore diameter assessed using the BJH method (Fig. 13): the pore size tended to decrease mainly by increasing the Al concentration -and thus the content of amorphous phase – and, to a minor extent, by decreasing the B concentration. It is worth mentioning however that, whatever the Al and B concentrations, the mean pore diameter of the pastes investigated in this work was always much smaller than that (138 Å) of the paste prepared in [16] with similar formulation parameters except for the mixing solution which also contained zinc cations.

3.3.4. *Multicriteria optimization*

To be used for waste conditioning, cement-based materials have to meet a number of quality demands depending on their elaboration process, but also on their subsequent storage in a repository. General requirements may include in particular a setting time ideally comprised between 5 h and 24 h (to avoid any risk of setting in the mixer in case of technical hitch, while keeping a good output of the conditioning unit), a rise in temperature resulting from cement hydration that does not affect the package integrity and a compressive strength higher than 20 MPa.

The time corresponding to the maximum heat flow giving a good estimation of the setting time, the results showed that to get setting in less than 24 h, mixing solutions with a small concentration of aluminum and a large concentration of boron should be avoided. However, such conditions would be interesting to get a low heat flow and a high cumulative heat (corresponding to a significant progress of hydration). Finding a compromise will then be necessary to meet the demands of not too long setting, limited self-heating and high progress of reaction within the first days after mixing.

A multi-criteria optimization [28–30] was performed to point out the compositions of the mixing solution making it possible to produce brushite cement-based materials checking these requirements. The fitted regression models were used to define individual desirability functions for responses t_{max}, HF_{max} and R_c. Every calculated response y_i was transformed into a d_i value, comprised between 0 and 100%, that represented the satisfaction level associated to the response value depending on the requirements. d_i was set to 100% if the calculated response value was equal to the target, and to 0 if it was outside the tolerance interval. Fig. 15 shows the individual desirability functions defined for the 3 investigated responses. Overall desirability function D was calculated as the geometric mean of the 3 individual desirability functions (Eq. (4)).

$$D = \sqrt[3]{d_1 \cdot d_2 \cdot d_3} \tag{4}$$

D was plotted as a function of the Al and B concentrations in the mixing solution (Fig. 16). The maximum value, corresponding to a satisfaction level of 98%, was obtained for Al and B concentrations of 2.1 mol·L^{-1} and 0.56 mol·L^{-1} respectively (R_c = 46.8 MPa, t_{max} = 25.7 h and HF_{max} = 4,97 mW·g^{-1}). The time for maximum heat flow slightly exceeded 24 h. More generally, function D took interesting values (above 90%) when the Al and B concentrations were within the ranges [1.8; 2.4 mol·L^{-1}] and [0.45; 0.6 mol·L^{-1}] respectively.

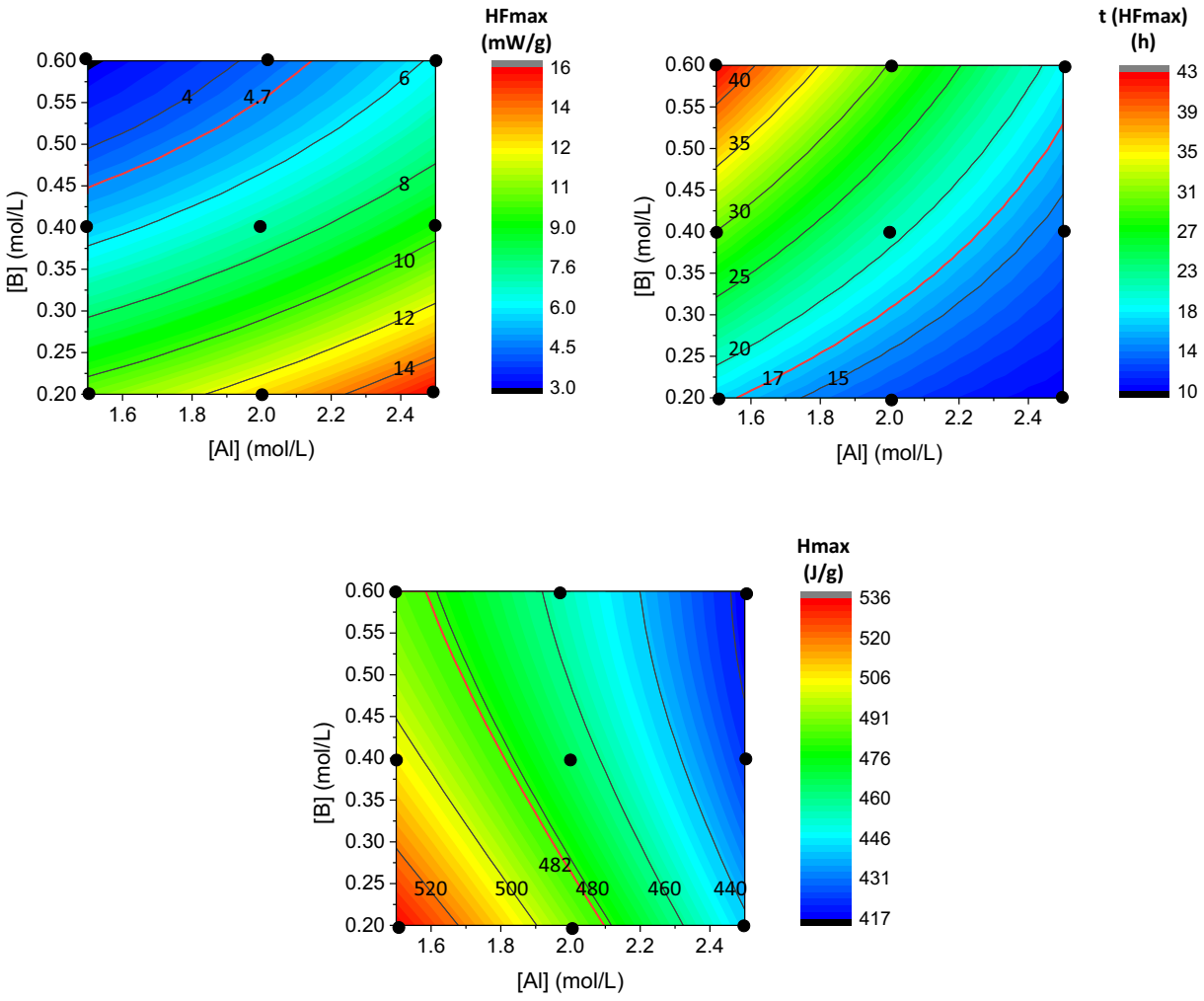

Fig. 10. HF_{max}, t_{max} and H_{max} contour plots in {[Al], [B]} plane. The red line corresponds to values obtained for a commercial binder investigated in [16]. (For interpretation of the references to colour in this figure legend, the reader is referred to the web version of this article.)

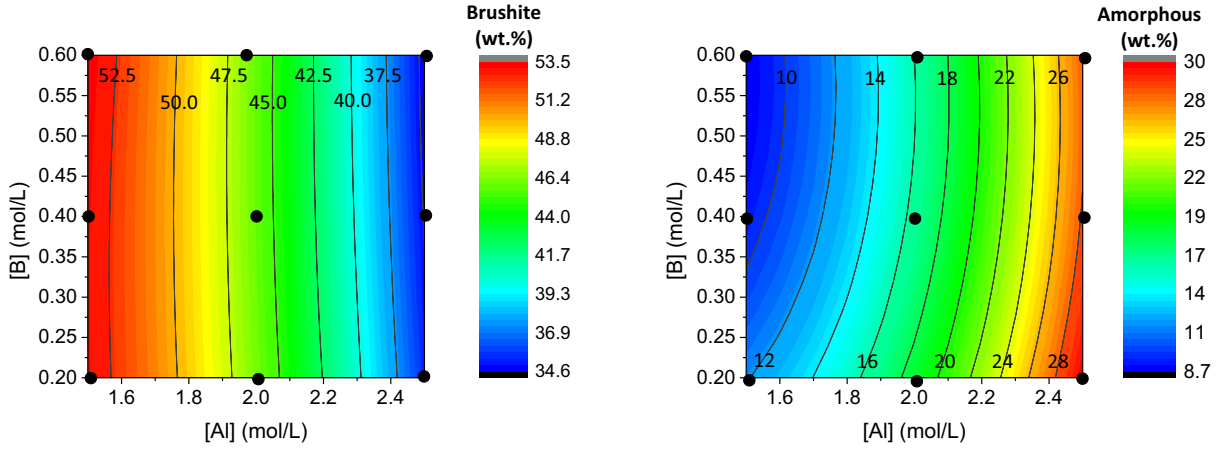

Fig. 11. Response contour plots for the mass fractions of brushite (left) and amorphous phase (right) in 28 d-old cement pastes (curing in sealed bag).

4. Conclusion

The mixing solution of wollastonite-based brushite cement usually contains orthophosphoric acid, borax or boric acid, and metallic cations (such as Zn^{2+} or Al^{3+}). However, data about the optimal composition and the role of each component are very limited. After a first study dedicated to the influence of the Ca/P molar ratio, H_3PO_4 initial concentration and l/s weight ratio [17], the focus was placed in this work on the separate and joint effects of boron and aluminum. The main conclusions can be summarized as follows.

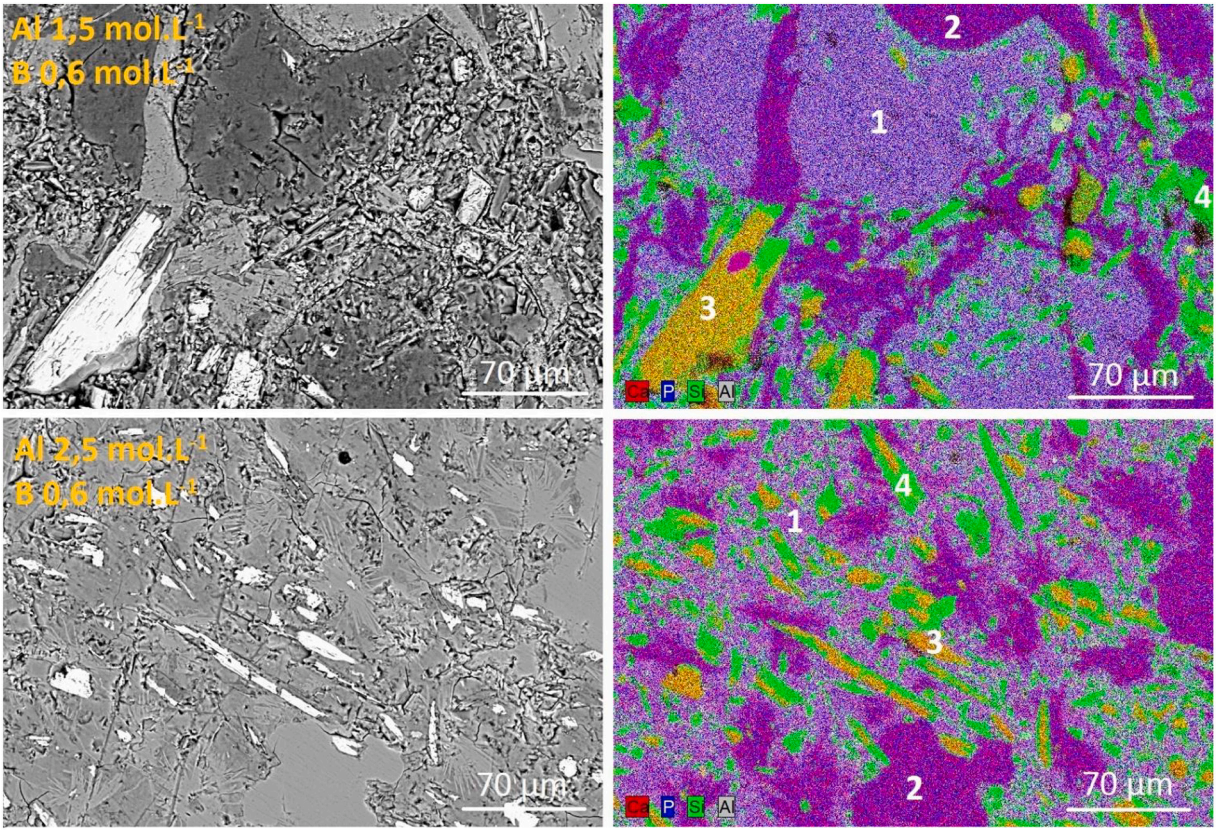

Fig. 12. Microstructure of 28 d-old paste samples $P_{B/0.6/1.5}$ and $P_{B/0.6/2.5}$ (mixing solution comprising 0.6 mol·L^{-1} B and 1.5 or 2.5 mol·L^{-1} Al): SEM images (backscattered electrons – polished cross section) and elemental mapping. 1: amorphous alumino-phosphate phase; 2: brushite; 3: wollastonite and 4: amorphous silica.

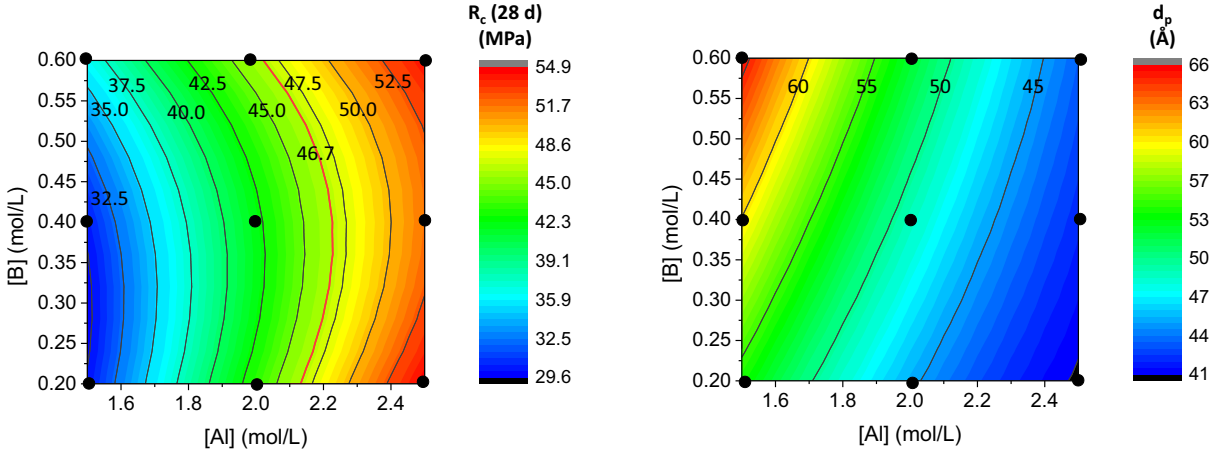

Fig. 13. Response contour plots for compressive strength (left) and mean mesopore diameter (BJH) (right) of 28 d-old cement pastes (curing in sealed bag).

1. Whatever the type of addition (borax or boric acid), boron retards the cement hydration process and makes it possible to strongly reduce the self-heating of the material. As a consequence, brushite precipitates instead of monetite.
2. Adding Al^{3+} cations to the mixing solution is necessary to get significant mechanical strength of hardened cement pastes. Precipitation of an amorphous alumino-phosphate phase seems to play a key role in the hardening process. Increasing the Al concentration also reduces the maximum heat flow and promotes the precipitation of brushite instead of monetite. However, it strongly reduces the duration of the low thermal activity period and setting times can become too short for field application.
3. The joint addition of boron and aluminum in the mixing solution is thus beneficial. High compressive strengths can be achieved thanks to the presence of aluminum while boron makes it possible to control the hydration rate, and thus the setting time. Empirical polynomial models have been built to predict several paste properties (maximal heat flow and corresponding hydration time, maximum cumulative heat, phase content and compressive strength at 28 d) as a function of the Al and B concentrations in the mixing solution. These models have then been used for multicriteria optimization: to design a

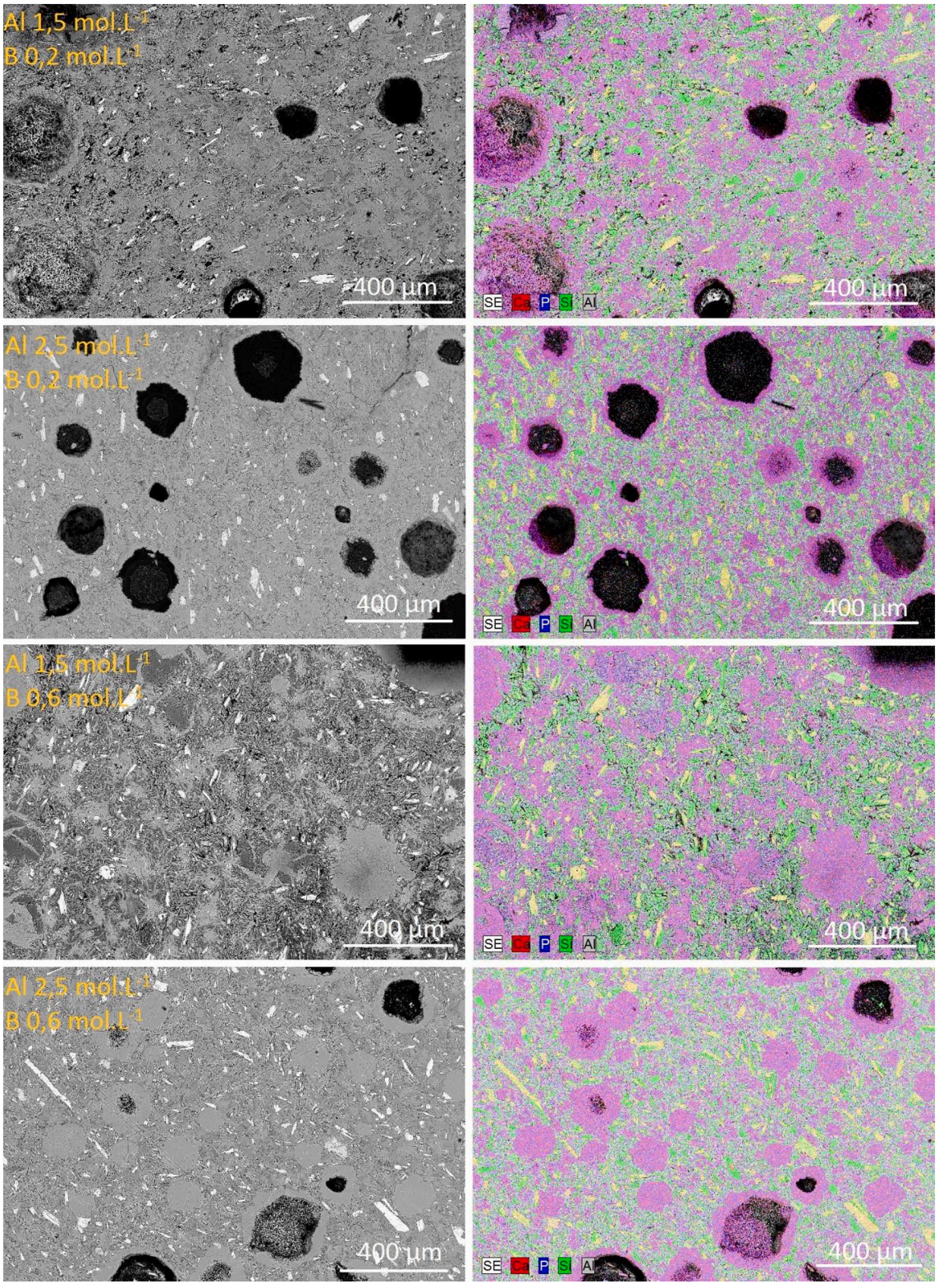

Fig. 14. Microstructure of 28 d-old paste samples $P_{B/0.2/1.5}$, $P_{B/0.2/2.5}$ $P_{B/0.6/1.5}$ and $P_{B/0.6/2.5}$ (mixing solution comprising 0.2 or 0.6 mol·L^{-1} B and 1.5 or 2.5 mol·L^{-1} Al): SEM images (backscattered electrons – polished cross section) and EDS elemental mapping.

conditioning matrix for waste stabilization / solidification, the B and Al concentrations should advantageously lie within the ranges [0.45; 0.6 mol·L^{-1}] and [1.8; 2.4 mol·L^{-1}] respectively.

4. As compared to previous work [16], it is possible to prepare a wollastonite-based brushite cement paste using a simplified mixing solution (without zinc) and obtain good properties both in the fresh and hardened states. Future work should focus on the long-term evolution of such material under the environment of a repository.

Declaration of competing interest

The authors declare that they have no known competing financial

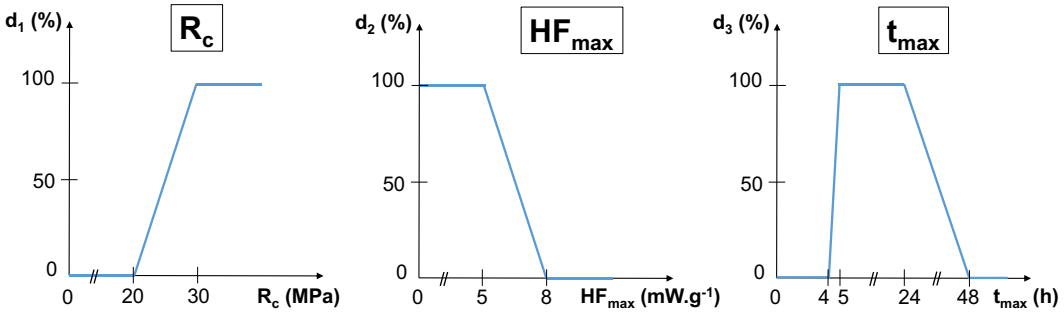

Fig. 15. Individual desirability functions for the compressive strength, maximum heat flow and corresponding hydration time.

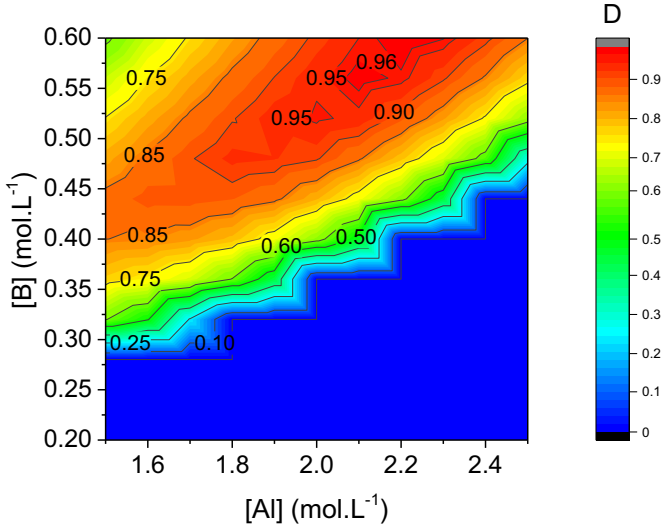

Fig. 16. Contour plot of overall desirability function D.

interests or personal relationships that could have appeared to influence the work reported in this paper.

Acknowledgements

Acknowledgements are due to Pascal Antonucci for his help in the laboratory.

References

[1] M. Atkins, F.P. Glasser, Application of Portland cement-based materials to radioactive waste immobilization, Waste Manag. 12 (1992) 105–131.
[2] Improved cement solidification of low- and intermediate-level radioactive waste, in: IAEA Technical Report Series No. 350, 1993.
[3] F. Glasser, Fundamental aspects of cement solidification and stabilisation, J. Hazard. Mater. 52 (1997) 151–170.
[4] M. Ojovan, W. Lee, S. Kalmykov, An Introduction to Nuclear Waste Immobilization, 3rd edition, Elsevier, Amsterdam, Netherlands, 2019, p. 512.
[5] B. Lothenbach, F. Winnefeld, C. Alder, E. Wieland, P. Lunk, Effect of temperature on the pore solution, microstructure and hydration products of Portland cement pastes, Cem. Concr. Res. 37 (2007) 483–491.
[6] E. Coppens, C. Cau Dit Coumes, P. Antonucci, On the immobilization of $NaNO_3$-rich ILW-LL radioactive effluent, in: Proc. NUWCEM 2014, 3–6 juin, Avignon, France, 2014.
[7] N.C. Collier, N.B. Milestone, J. Hill, H. Godfrey, Immobilisation of Fe Floc: part 2, encapsulation of floc in composite cement, J. Nucl. Mater. 393 (2009) 92–101.
[8] B. Fournier, M.A. Berube, Alkali-aggregate reaction in concrete: a review of basic concepts and engineering implications, Can. J. Civ. Eng. 24 (2000) 167–191.
[9] N. Courtois, C. Cau Dit Coumes, A. Poulesquen, J. Haas, S. Ben Hadj Hassine, D. Bulteel, Rheological and swelling properties of alkali-silica gels produced in cemented waste packages, in: Proc. Intern. Conf. Cem. Chem., 15th ICCC, Prague, Czech Republic, September 16–20, 2019.
[10] C. Cau Dit Coumes, Alternative binders to ordinary Portland cement for radwaste solidification and stabilization, in: F. Bart, C. Cau Dit Coumes, F. Frizon, S. Lorente (Eds.), Cement-based Materials for Nuclear Waste Storage, Springer, New-York, 2012, pp. 171–192.
[11] C.E. Semler, Lime Silico Phosphate Ceramics, The United States Department of Transportation, Washington DC, USA, 1974 (p 6 3,804,661).
[12] C.E. Semler, A quick-setting wollastonite phosphate cement, Ceram. Bull. 55 (1976) 983–988.
[13] G. Mosselmans, M. Biesemans, R. Willem, J. Wastiels, M. Leermakers, H. Rahier, S. Brughmans, B. Van Mele, Thermal hardening and structure of a phosphorus containing cementitious model material, J. Therm. Anal. Calorim. 88 (2007) 723–729.
[14] X. Wu, J. Gu, Inorganic Resins Composition, Their Preparation and Use Thereof, Vrije Universiteit Brussel, Belgium, 2000, p. 15. EP 0 861 216 B1.
[15] M. Alshaaer, H. Cuypers, G. Mosselmans, H. Rahier, J. Wastiels, Evaluation of a low temperature hardening inorganic phosphate cement for high-temperature applications, Cem. Concr. Res. 41 (2011) 38–45.
[16] P. Laniesse, C. Cau Dit Coumes, A. Poulesquen, A. Bourchy, A. Mesbah, G. Le Saout, P. Gaveau, Setting and hardening process of a wollastonite-based brushite cement, Cem. Concr. Res. 106 (2018) 65–76.
[17] P. Laniesse, C. Cau Dit Coumes, A. Mesbah, G. Le Saout, Understanding the setting and hardening process of wollastonite-based brushite cement. Part 1: influence of the Ca/P ratio and H_3PO_4 concentration of the mixing solution, Cem. Concr. Res. 134 (2020) 106094.
[18] L.P. Hammett, A.J. Deyrup, A series of simple indicators, J. Am. Chem. Soc. 54 (1932) 2721–2739.
[19] D.C. Montgomery, Design and Analysis of Experiments, 5th ed., John Wiley & Sons, Hoboken, USA, 2001 (684 p.).
[20] G.E.P. Box, K.B. Wilson, On the experimental attainment of optimum conditions, J. R. Stat. Soc. B 13 (1951) 1–45.
[21] C. Frontera, J. Rodriguez-Carvajal, FullProf as a new tool for flipping ratio analysis, Phys. B 335 (2003) 219–222.
[22] M. Alshaaer, H. Cuypers, H. Rahier, J. Wastiels, Production of monetite-based Inorganic Phosphate Cement (M-IPC) using hydrothermal post curing (HTPC), Cem. Concr. Res. 41 (2011) 30–37.
[23] E.J. Weisshart, J.D. Rimstidt, Wollastonite: incongruent dissolution and leached layer formation, Geochim. Cosmochim. Acta 64 (2000) 4007–4016.
[24] E. Green, A. Luttge, Incongruent dissolution of wollastonite measured with vertical scanning interferometry, Am. Mineral. 91 (2006) 430–434.
[25] N.R. Draper, H. Smith, Applied Regression Analysis, 3rd ed., John Wiley&Sons, New York, 1998 (706 p).
[26] D. Mathieu, J. Nony, R. Phan Tan Luu, NEMROD-W Version 2015, LPRAI, Marseille, France.
[27] H.E. Lundager Madsen, Influence of foreign metal ions on crystal growth and morphology of brushite ($CaHPO_4.2H_2O$) and its transformation to octacalcium phosphate and apatite, J. Cryst. Growth 310 (2008) 2602–2612.
[28] E.C. Harrington Jr., The desirability function, Ind. Qual. Control. 21-10 (1965) 494–498.
[29] G. Derringer, R. Suich, Simultaneous optimization of several response variables, J. Qual. Technol. 12 (1980) 214–219.
[30] A.I. Khuri, M. Conlon, Simultaneous optimization of multiple responses represented by polynomial regression functions, Technometrics 23 (1981) 363–375.